Biosensors and Bioelectronics 126 (2019) 301–307

Contents lists available at ScienceDirect

Biosensors and Bioelectronics

journal homepage: www.elsevier.com/locate/bios

Development of a multiplexed giant magnetoresistive biosensor array prototype to quantify ovarian cancer biomarkers

Todd Klein[a], Wei Wang[a], Lina Yu[a], Kai Wu[a], Kristin L.M. Boylan[b], Rachel Isaksson Vogel[c], Amy P.N. Skubitz[b,c,1], Jian-Ping Wang[a,*,1]

[a] Department of Electrical and Computer Engineering, University of Minnesota, Minneapolis, MN 55455, USA
[b] Department of Laboratory Medicine and Pathology, University of Minnesota, Minneapolis, MN 55455, USA
[c] Department of Obstetrics, Gynecology, and Women's Health, University of Minnesota, Minneapolis, MN 55455, USA

ARTICLE INFO

Keywords:
Giant magnetoresistance
Ovarian cancer
Multiplex detection
Biomarkers
Hand-held system
CA125
HE4
IL6

ABSTRACT

In this work, we developed benchtop and handheld Giant Magnetoresistive (GMR) biosensing systems that serve as platforms for detecting a wide variety of protein biomarkers for human diseases. System development included spintronic and nanomagnetic materials, biomolecular chemistry, electronic circuitry, analog and digital signal processing, firmware programming, user interface programming on both PC and Android smartphone, communications over both USB and Bluetooth, and mechanical integration. In this work, we demonstrated the benchtop GMR biosensing system in the context of ovarian cancer assay development. The prototype system delivered the required performance in terms of high-sensitivity multiplex assays in a portable format with enough flexibility to serve as a platform for ovarian cancer and many other diseases. We achieved multiplex detection of cancer antigen 125 (CA125 II), human epididymis protein 4 (HE4), and interleukin 6 (IL6), with limits of detection (LOD) as low as 3.7 U/mL, 7.4 pg/mL, and 7.4 pg/mL, respectively.

1. Introduction

Early disease detection is an important factor in effective medical treatment and better patient outcomes. Technologies that facilitate early detection of disease provide a path toward less expensive, more effective, and sustainable healthcare. Protein biomarker quantification has been proposed as a potential method of screening for many diseases (Goh et al., 2016; Li et al., 2010; Makawita and Diamandis, 2010; Rifai et al., 2006; Rossetti et al., 2017), but stringent requirements must be met for clinical screening and subsequent early detection. Although ovarian cancer is not the most common cancer, it is particularly insidious due to the lack of recognizable early symptoms (Jayson et al., 2014; Matz et al., 2017; Oza et al., 2015). In the United States, over 22,000 women are newly diagnosed with ovarian cancer each year, and over 14,000 women die from the disease (Siegel et al., 2016) largely due to its late stage at the time of disease diagnosis (Jayson et al., 2014). Current treatments are most effective when ovarian cancer is detected in its early stages; thus, early detection is key to long-term survival.

To date, no ovarian cancer biomarker assay has been produced with adequate clinical sensitivity and specificity to be FDA approved for ovarian cancer screening in the general population (Su et al., 2013; Ueland, 2017; Yang et al., 2017). To be useful for wide-spread screening, the optimal technology is required to be small, affordable, fully automated, and with the sensitivity and precision of central laboratory equipment while measuring concentrations of multiple biomarkers simultaneously (i.e., multiplex).

GMR biosensing technology has advantages such as high sensitivity, low cost, real-time signal readout, and compatibility with the modern integrated circuits (IC) (Costa et al., 2017). This technology has been applied for the detection of nucleic acids (Dias et al., 2016; Zhi et al., 2012), protein biomarkers (Choi et al., 2016; Krishna et al., 2016; Srinivasan et al., 2011; Wang et al., 2015; Wu et al., 2017), bacteria (Barroso et al., 2018), and metal ions (Wang et al., 2014). By combining GMR biosensors with high moment magnetic nanoparticles (MNPs) such as FeCo, higher sensitivities are observed (Jing et al., 2009; Srinivasan et al., 2009). In relation to optical biosensing technologies, GMR biosensing has some inherent advantages including matrix insensitivity (Gaster et al., 2009) and the potential for high sensitivity multiplex assays in a portable instrument. Multiplexing is quite natural in GMR biosensing simply because the magnetic dipole fields remain localized near each sensor surface and therefore do not interfere with

* Corresponding author.
E-mail address: jpwang@umn.edu (J.-P. Wang).
[1] These two authors are joint senior authors on this manuscript.

https://doi.org/10.1016/j.bios.2018.10.046
Received 2 September 2018; Received in revised form 21 October 2018; Accepted 22 October 2018
Available online 23 October 2018
0956-5663/

neighboring sensors. These attributes make GMR biosensors versatile and strong candidates for future high performance molecular diagnostic applications.

In this work, we focus on the effort to provide a tool for early detection of ovarian cancer. We developed benchtop and hand-held versions of our giant magnetoresistive (GMR) biosensing system and conducted initial testing of three biomarkers (CA125 II, HE4, and IL6) that are well established in the literature to be present at elevated levels in the sera of women with late stage high grade serous ovarian cancer (Moore et al., 2009). Our initial demonstration uses a cocktail of CA125 II, HE4, and IL6 in phosphate buffered saline (PBS) with various concentrations of each analyte for a multiplex measurement on a benchtop version of our GMR biosensing system. The long-term goal of this research is to develop a low-cost, easy-to-use, highly sensitive test for the detection of ovarian cancer in its early stages when treatments are most effective, as well as for detection of disease recurrence.

2. Materials and methods

2.1. GMR sensors

Each fabricated GMR chip was 15 mm × 15 mm in size (see Fig. 1A) and contained one reaction well which allowed for a one-time-use multiplexed immunoassay. In each reaction well, there were 4 groups of 4 × 4 GMR sensor arrays, with one group selected for this study based on preferred fabrication parameters (Fig. 1B–C). Other groups of sensors were unused for this work. Each GMR sensor in the selected group had an overall sensing area of 100 μm × 150 μm (Fig. 1D). Each GMR sensor was composed of 5 groups of GMR strips connected in series and separated by a 3 μm pitch. Each group contained 10 GMR strips connected in parallel (Fig. 1D). Fabricated strip widths of 750 nm were confirmed by a JOEL 6700 scanning electron microscope (SEM) (Fig. 1E–F).

2.2. GMR sensor surface bio-modification

The GMR sensors were capped with SiO_2 which served two functions: (i) as a protective layer to prevent corrosion by any chemicals or biological samples, and (ii) to provide free hydroxyl groups for subsequent bio-modifications. Before the sensor surface bio-modification process, each GMR chip was triple-washed with 100% acetone, 100% methanol, and 100% isopropyl alcohol, dried, and then placed under ultraviolet light and ozone (UVO) for 15 min to remove organic contaminants. Subsequently, each GMR chip was soaked in 1% 3-aminopropyltriethoxysilane (APTES) in anhydrous toluene for 15 min to allow the chemical binding of APTES to free hydroxyl groups from SiO_2. Afterwards, each GMR sensor array area was covered with 50 μL 5% glutaraldehyde (Glu) in deionized (DI) water for 5 h to allow the chemical binding between aldehyde groups (from Glu) and amino groups (from APTES) (Krishna et al., 2016; Wang et al., 2013, 2015; Wu et al., 2017). The other aldehyde group on Glu allowed the subsequent binding of capture antibodies or bovine serum albumin (BSA). Functionalization with capture antibodies was performed with a piezo dispense capillary (PDC) using a programmable liquid dispensing system (sci-FLEXARRAYER S5, Scienion, Germany) (see Fig. 1G).

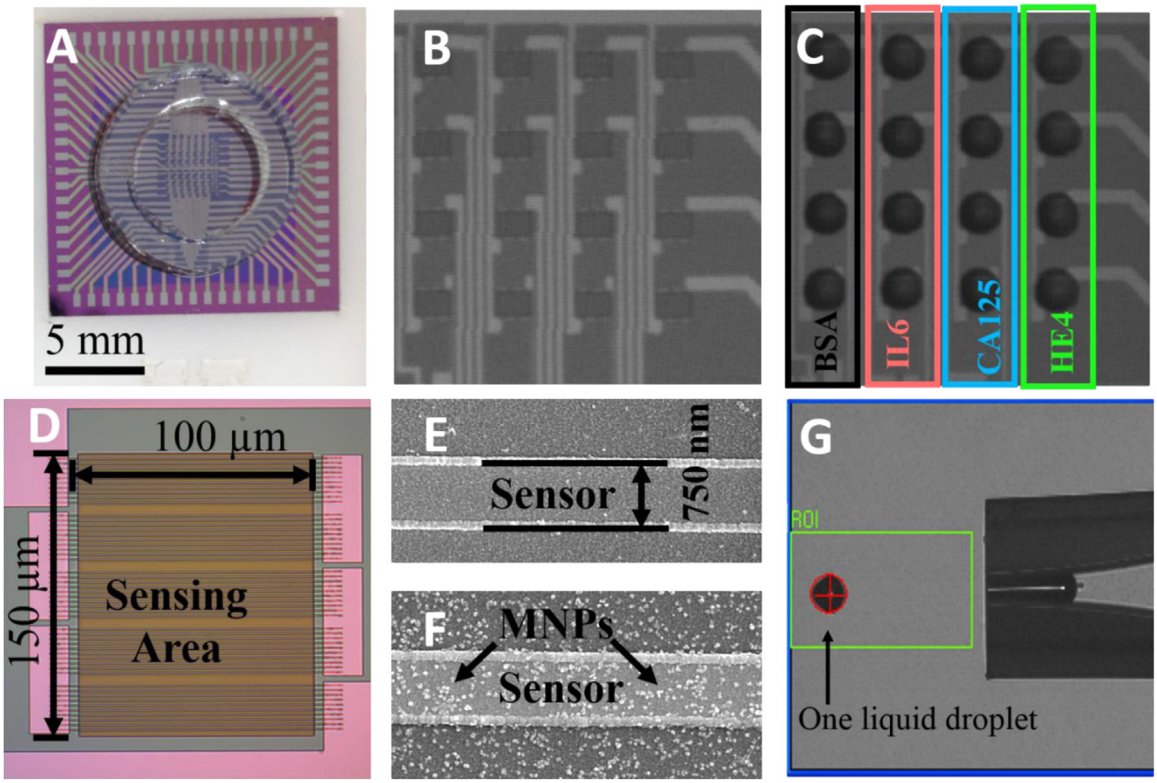

Fig. 1. (A) One-time-use GMR biosensing chip with the size comparable to a U.S. 10 cent coin. (B) Photomicrograph of the GMR sensor array in the reaction well. For each trial, we used a 4 × 4 active GMR sensor array in each reaction well, resulting in a total of 16 GMR sensors. (C) Photomicrograph of the GMR sensor array after spotting with CA125 II capture antibody, HE4 capture antibody, IL6 capture antibody, and bovine serum albumin (BSA) on each column. Each GMR sensor was completely covered with 1.2 nL of capture antibodies (500 μg/mL) or BSA (10 mg/mL). (D) Each GMR sensor consisted of 5 sensor groups connected in series, and each sensor group consisted of 10 GMR sensor strips connected in parallel. (E) SEM image of one GMR sensor strip with the width of 750 nm. (F) SEM image of GMR sensor strip after completion of the immunoassay. Magnetic beads were evenly bound to sensor surface. (G) A piezo dispense capillary (PDC) was capable of dispensing 400 pL of liquid droplet onto target area. In this study, each GMR sensor was spotted with 3 droplets of capture antibodies or BSA.

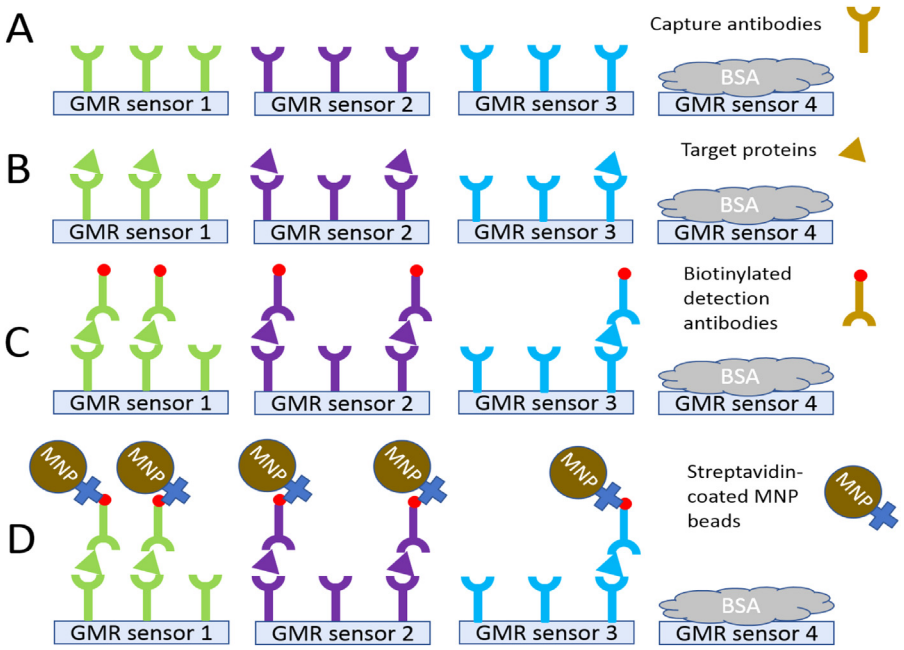

Fig. 2. Assay sequence: (A) four groups of GMR sensors were spotted with either capture antibodies against CA125 II (green on GMR sensor 1), HE4 (purple on GMR sensor 2) and IL6 (blue on GMR sensor 3) or BSA (gray on GMR sensor 4) to define the function of each sensor. (B) Sensors were incubated with a sample that contained a mixture of the target proteins (CA125 II, HE4, and IL6) which selectively bound to capture antibodies. (C) Sensors were incubated with biotinylated detection antibodies which selectively bound to each specific target protein. (D) GMR signals were monitored while incubated with streptavidin-coated ads (see Supplementary information S1) (For interpretation of the references to color in this figure legend, the reader is referred to the web version of this article.).

2.3. Multiplex fluorescent immunoassay

We first validated the multiplex immunoassay on a glass slide from Surmodics and measured in a Genepix fluorescent scanner. The results were used to optimize and verify a variety of aspects in the assay including capture antibody concentrations, detection antibody concentrations, and interference of each component within the multiplex assay.

2.4. GMR sensor array based multiplex immunoassay

The GMR biosensor assay sequence described above is illustrated in Fig. 2. Multiplex GMR biosensor experiments were performed with antibodies against three different target proteins on a single chip. A negative control of BSA (10 mg/mL) along with three capture antibodies (CA125 II, HE4, and IL6; each at 500 μg/mL) were robotically spotted onto individual sensors in replicates of four. A total of 16 sensors were used during each multiplex experiment. Using the programmable liquid dispensing system, a spotting volume of approximately 1.2 nL completely covered the sensor. Incubation for 24 h at a temperature of 4 °C and approximately 90% relative humidity was performed to immobilize capture antibodies on the GMR surface. After being rinsed with an immunoassay stabilizer (SC01–1000, Surmodics) three times to remove unbound capture antibodies, the chip was washed with PBST (PBS containing 0.05% Tween 20), then DI water, and then dried with nitrogen gas. A laser-cut acrylic ring was attached to the GMR chip surface with silicone adhesive (SYLGARD 184) forming a reaction well to contain fluids while they incubated over the sensor surface. A blocking buffer containing BSA was added and incubated for one hour to block unbound surface sites. The blocking buffer was then removed, and the chip was washed with PBST buffer.

PBST was spiked with 100 μL mixtures of CA125 II, HE4, and IL6 in PBS at a variety of concentrations and incubated over the sensor surface for 60 min at room temperature to allow the specific binding between target proteins and capture antibodies. The sensors were then washed with PBST buffer. The three biotinylated detection antibodies for CA125 II, HE4, and IL6, each at a concentration of 5 μg/mL PBS (total mixture volume of 100 μL), were then added to the reaction well and incubated at room temperature for 60 min. Finally, the chip was washed with PBST and dried with nitrogen gas.

2.5. Magnetic beads selection

Magnetic beads are a collection of superparamagnetic MNPs in a matrix of polymer or other nonmagnetic material. Selection of magnetic beads for GMR biosensing depends on MNP size and material, bead size, and surface chemistry. If MNP size is too large, then they will not be superparamagnetic. If the material used for MNPs has high saturation magnetization, then we can achieve higher signals with small MNP size (Jing et al., 2009; Srinivasan et al., 2009; Wang et al., 2015). If beads are too small, the beads may be difficult to detect. If too large, the beads may quickly settle out of solution.

Surface chemistry affects beads' specific and non-specific binding. For example, the beads and sensor surface can either repel or attract depending on the relative polarity and magnitude of surface charge. If they strongly repel, then this can interfere with specific binding in the assay. If they strongly attract, then this can contribute to non-specific binding. Thus, the characteristic of surface charge for beads should be also considered depending on target analytes and detection technique.

The magnetic beads used in this experiment were Ademtec 200 nm beads. Each bead was composed of approximately 1000 MNPs with an averaged estimated magnetic moment of 2.3×10^{-16} emu, held together by a polymer matrix. Vibrating sample magnetometer (VSM) data and analysis of the Ademtec beads can be found in Supplementary information S2. These beads were selected for high magnetic volume and therefore high moment per bead binding event. One drawback of using such large beads was the potential of non-specific signal due to beads settling out of solution. For this reason, we included a negative control group blocked with BSA to subtract the background signal.

2.6. Electrical circuit and signal generation

A simplified schematic representation of the electrical circuit is illustrated in Fig. 3A. Channel A of a 24-bit stereo audio CODEC drove a frequency f_1 at the top of a nearly-balanced Wheatstone Bridge circuit with a GMR biosensor in one of the four resistor locations. Each sensor was addressed through an analog switch multiplexer. Prior to testing, all the sensors were individually balanced against a resistance ladder. This ensured that the electronics were flexible enough to work with a range of sensor resistances even on a single biosensor chip. Channel B of the CODEC was routed to a voltage-controlled current source that drove a coil at frequency f_2.

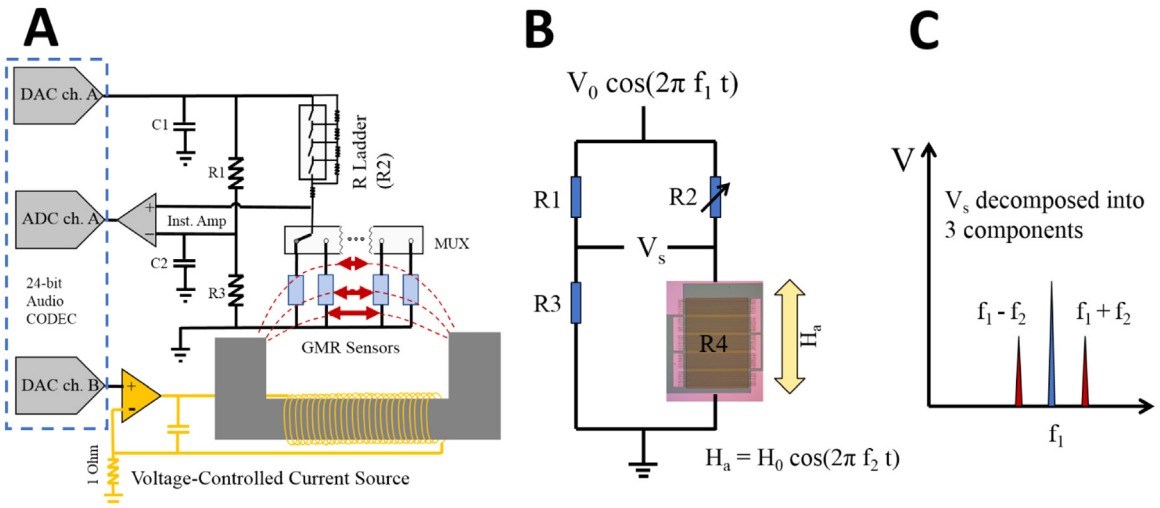

Fig. 3. (A) Schematic representation of Wheatstone Bridge circuit on the multiplexing board. (B) Simplified schematic of Wheatstone Bridge. (C) Signal decomposed into a center tone and two mixed frequency components (side tones). The two side tones (f_1 +/- f_2) represent the signals that change in response to the capture of MNPs through the sandwich assay structure.

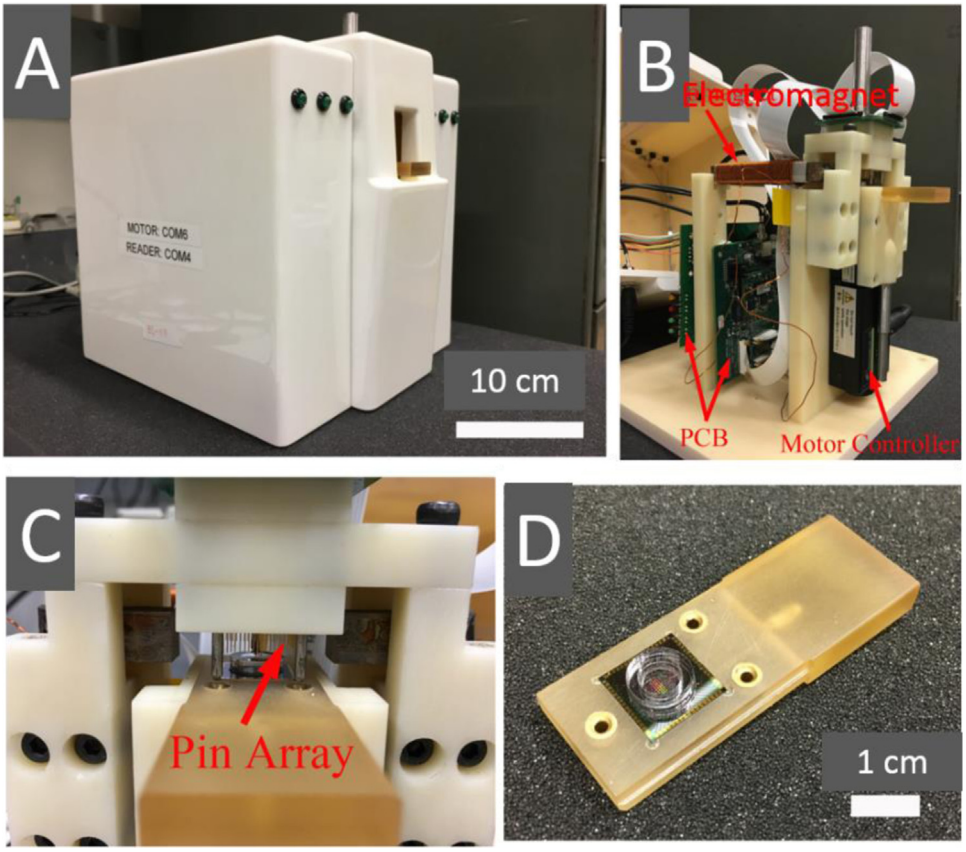

Fig. 4. (A) Benchtop GMR base station, with an overall size of 20 cm × 20 cm × 20 cm. (B) Design inside the base station including two printed circuit boards (PCBs) to communicate with the motor and monitor sensors. (C) Pin array aligning and moving close with the electrode pads of the GMR chip. (D) Reaction-well attached GMR chip on the chip holder.

In Fig. 3B–C, the bridge drive frequency f_1 mixed with the coil drive frequency f_2 due to resistance modulation in the GMR on the sensing side of the bridge (De Boer et al., 2007; Hall et al., 2010). The three resulting signals at frequencies f_1 (center tone) and f_1 + /- f_2 (side tones) were balanced against two reference resistors on the other side. Appropriate balance was achieved by tuning the resistance ladder for each individual sensor prior to the measurement. Since the reference resistors did not modulate frequency, they only produced a signal at the center tone. Subtraction and amplification of Wheatstone Bridge voltages occurred at the instrumentation amplifier. The resulting signal contained a relatively small amount of power at the center tone frequency due to bridge balance. Consequently, we could amplify the side tones significantly above system noise at the analog-to-digital converter (ADC).

The performance of the circuit was judged in terms of signal-to-noise ratio (SNR) of the center tone GMR sensors which is approximately 100 dB. The center tone was selected for this purpose because it is primarily limited by the circuit components and signal processing whereas SNR of the side tones is highly dependent on the magnetoresistance of sensors. The side tone SNR was approximately 75 dB for the GMR sensors and benchtop system used in this work.

After converting the signal to digital data, we performed a Fourier

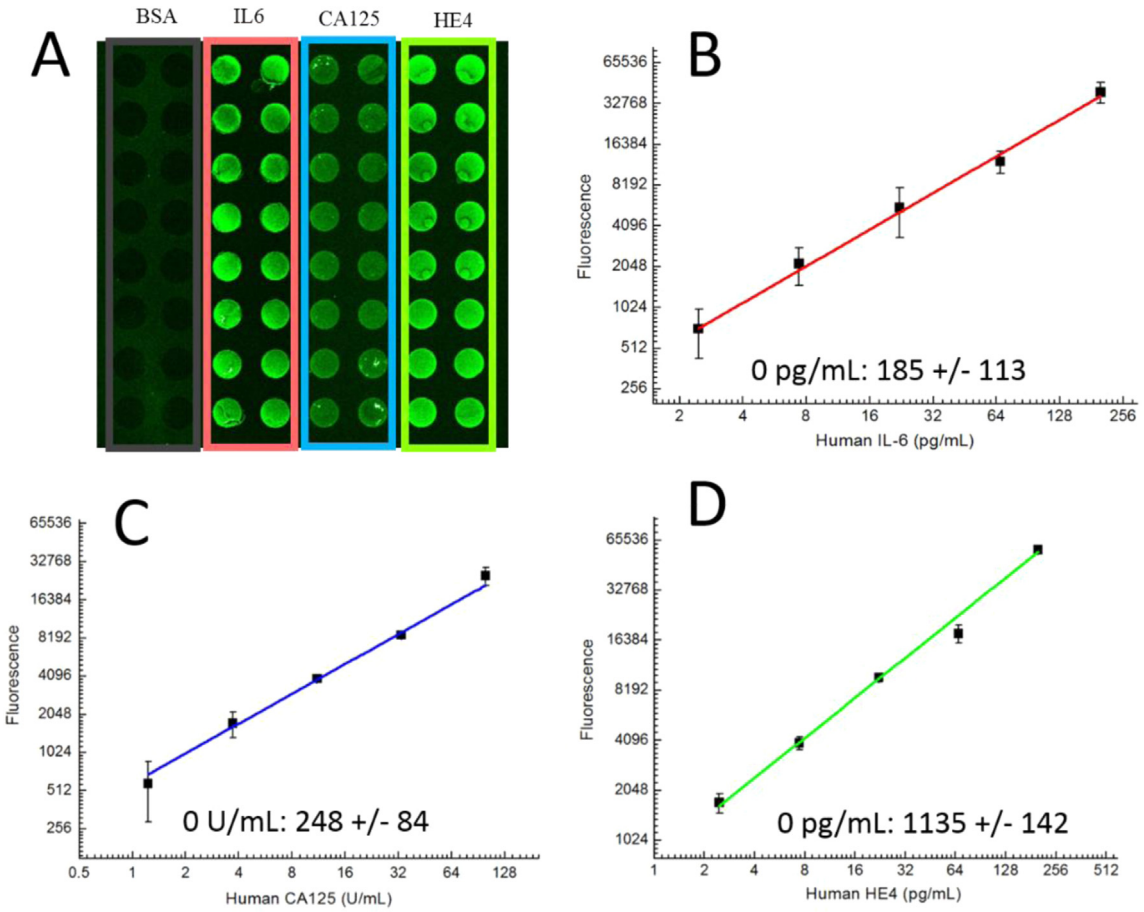

Fig. 5. (A) A mixture of IL6, CA125 II, and HE4 of different concentrations in PBS was measured by the fluorescence assay. The concentrations of target proteins are: IL6: 66.7 pg/mL, CA125 II: 33.3 U/mL, HE4: 66.7 pg/mL. (B–D) Calibration curves of multiplexed IL6, CA125 II, and HE4 immunoassays. Error bars indicate standard deviations of the signals from different spots. Zero concentration data for each analyte is listed below each curve.

Transform at the center tone and side tone frequencies to monitor the amplitudes of each. By monitoring the side tones, we focused only on the portion of signal derived from the magnetic field and were therefore able to resolve the tiny changes induced by the MNPs.

The amplitude of the center tone was related to the resistance of the GMR sensor as it was balanced against the other three resistors of the Wheatstone Bridge. Tracking the side tones allowed us to monitor the signal of interest, while monitoring the center tone allowed us to validate the sensor stability in terms of temperature drift and leaky encapsulation. For example, if buffer solution leaked into the cracks of the encapsulation layer, we would see at least a partial short-circuit condition within the group of GMR strips defining the sensor. In that case, a sudden jump of center tone would be observed, and that sensor data would be removed from assay analysis.

2.7. Signal acquisition

The benchtop GMR base station as shown in Fig. 4 was used to collect multiplex ovarian cancer assay signals. The GMR chip was loaded into the benchtop GMR base station and 30 µL PBS was added to the reaction well. Following a 10-min warm-up period, we allowed the signal to generate a baseline for 3 min before adding the MNPs.

An identical circuit board was also integrated with a handheld version shown in Supplementary information S3 and S4. The handheld system signal was demonstrated for a positive control sample of biotin-BSA that can be found in Supplementary information S4.

3. Results and discussion

3.1. Multiplex detection of CA125 II, HE4, and IL6 with fluorescent assay

The purpose of the fluorescent assay was to verify the assay before moving to the GMR biosensor. We ran samples spiked with different permutations of the three proteins to confirm that the assays did not interfere. For example, one permutation with no signal (or too low for detection) was CA125 II capture antibodies and biotinylated CA125 II detection antibodies tested against HE4 proteins, (see Fig. 2A–C). Another similar permutation was the same CA125 II antibodies tested against IL6 proteins. We also tested a sample of buffer that had no additional proteins to confirm that detection antibodies did not bind directly to capture antibodies of the same assay. The results indicated low interference, and that BSA was an effective blocking agent.

To validate this multiplex immunoassay scheme, we carried out the multiplex fluorescence assay first. Different mixtures of CA125 II, HE4, and IL6 in PBS were incubated on the glass slides from Surmodics and the fluorescence signals were scanned by the Genepix fluorescent scanner. Fig. 5(A) shows the fluorescence image from one mixture of CA125 II, HE4, and IL6. Fig. 5(B–D) show the calibration curves of multiplex fluorescence assays on CA125 II, HE4, and IL6 respectively. Data for zero concentration is listed below each calibration curve. A low signal at zero concentration indicates minimal cross-reactivity between each variety of capture antibody and each variety of detection antibody (9 different combinations). The non-specific bonding was below the limit of detection for each assay. Additional testing was performed to ensure undetectable cross-reactivity between each target protein and

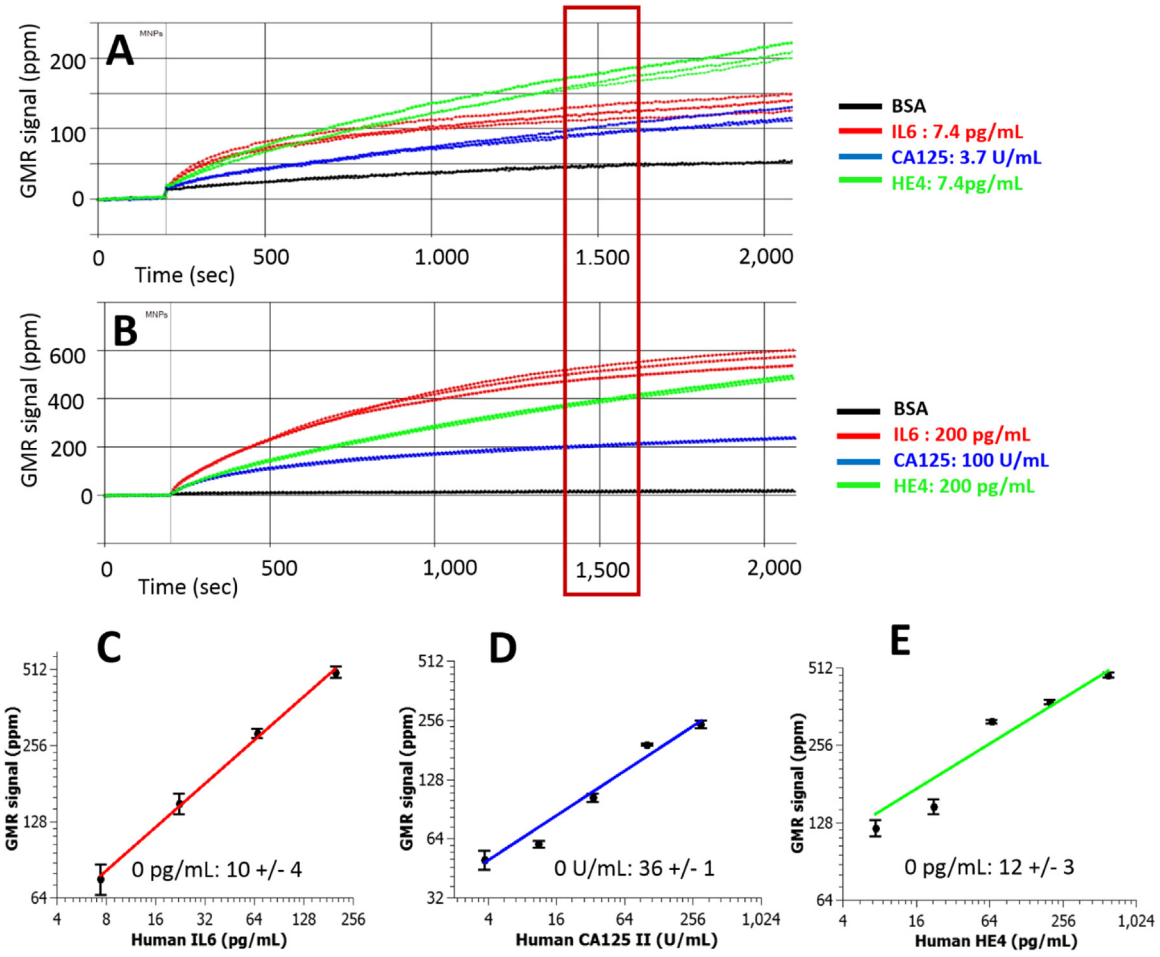

Fig. 6. (A–B) Real-time multiplex tests on GMR sensors. GMR signals for BSA (black), IL6 (red), CA125 II (blue), and HE4 (green), respectively. (A) IL6: 7.4 pg/mL, CA125 II: 3.7 U/mL, HE4: 7.4 pg/mL. (B) IL6: 200 pg/mL, CA125 II: 100 U/mL, HE4: 200 pg/mL. (C–E) Calibration curves of multiplexed IL6, CA125 II, and HE4 assays. Error bars indicate standard deviations of the signals from quadruplicate GMR sensors. Zero concentration data for each analyte is listed below each curve (For interpretation of the references to color in this figure legend, the reader is referred to the web version of this article.).

the other two assays.

3.2. Multiplex detection of IL6, CA125 II, and HE4 with GMR biosensor

Fig. 6(A and B) show the multiplexed, real-time magnetic response curves from two GMR bioassay measurements. Data points on each calibration curve represent 4 replicate GMR sensor signals on a chip. The various concentrations required to build each dose-response curve were attained by mixing all three target proteins at each specified concentration for each data point. The mixtures of target proteins were each incubated on separate GMR chips.

Fig. 6(C–E) show the calibration curves of IL6, CA-125, and HE-4 from our GMR biosensors, respectively. Due to the interpretation of zero-concentration data from the fluorescent version of this multiplex assay, we determined that non-specific signals on GMR were not from cross-reactivity between antibodies but instead due to beads settling out of solution and / or reactivity between capture antibodies and streptavidin-coated magnetic beads. This small non-specific signal was measured on the BSA-coated sensors and subtracted from all sensor data. The limits of detection were estimated to be 3 times the standard deviation of blank sample. Data for zero concentration were listed below each calibration curve in Fig. 6.

The dynamic range demonstrated for each protein concentration was two orders of magnitude. This was adequate for the detection of biologically relevant concentrations of the biomarkers, but somewhat limited on the upper end of concentration. On the low end, the limit of detection was less than 8 pg/mL for both HE4 and IL6 and less than 4 units/mL for CA125 II. These limits of detection are acceptable for medically relevant assays [26].

4. Conclusions

We achieved multiplex detection of cancer antigen 125 (CA125 II), human epididymis protein 4 (HE4), and interleukin 6 (IL6), with limits of detection (LOD) as low as 3.7 U/mL, 7.4 pg/mL, and 7.4 pg/mL, respectively. The system was constructed from a GMR biosensor array whose magnetoresistance signals were monitored by a nearly balanced (per each sensor) Wheatstone Bridge circuit. Each sensor can be printed with the desired capture antibodies to serve as selective binding sites for the biomarkers within the multiplex assay for simultaneous testing. Based on existing protein biomarker assays for ovarian cancer detection, the total number of biomarkers required for a multiplex assay is expected to be at least three. Exceeding this number of biomarkers would be desirable in a screening application, which will require extensive biological research to deliver the required sensitivity and specificity.

We believe that the GMR biosensor will contribute to ovarian cancer screening as soon as assays with appropriate sensitivity and specificity are developed. We have yet to see if the system can be affordable, fully automated, and able of competing with central laboratories in terms of

precision and reliability; development in those areas is currently underway. The total time for the assay in this demonstration was several hours due to long incubation times in the reaction well, but preliminary data with microfluidic integration shows similar results can be attained within a total time of 20–30 min. The long-term goal of this research is to develop a low-cost, easy-to-use, highly sensitive test for the detection of ovarian cancer in its early stages when treatments are most effective, as well as for detection of disease recurrence.

Acknowledgements

We acknowledge XPRIZE Foundation and Nokia Sensing XCHALLENGE competition for motivating the design of the z-Lab Diagnosis Platform which won a Distinguished Prize Award. This work was supported in part by an Ovarian Cancer Translational Pilot Award (W81XWH-11-1-0496) through the U.S. Department of Defense. Additional funding came both from the Jan Chorzempa Cancer Research Endowed Fund (11726) though the University of Minnesota Foundation and from a Doctoral Dissertation Fellowship through the University of Minnesota Graduate School. Parts of this work were carried out in the Characterization Facility, University of Minnesota, a member of the NSF-funded Materials Research Facilities Network (www.mrfn.org) via the MRSEC program.

Declaration of interest

Jian-Ping Wang has equity and royalty interests in, and serves on the Board of Directors and the Scientific Advisory Board, for Zepto Life Technology LLC, a company involved in the commercialization of GMR Biosensing technology. The University of Minnesota also has equity and royalty interests in Zepto Life Technologies LLC. These interests have been reviewed and managed by the University of Minnesota in accordance with its Conflict of Interest policies. Todd Klein is an employee and has equity in Zepto Life Technologies LLC.

Appendix A. Supporting information

Supplementary data associated with this article can be found in the online version at doi:10.1016/j.bios.2018.10.046.

References

Barroso, T.G., Martins, R.C., Fernandes, E., Cardoso, S., Rivas, J., Freitas, P.P., 2018. Biosens. Bioelectron. 100, 259–265.
Choi, J., Gani, A.W., Bechstein, D.J.B., Lee, J.-R., Utz, P.J., Wang, S.X., 2016. Biosens. Bioelectron. 85, 1–7.
Costa, T., Cardoso, F.A., Germano, J., Freitas, P.P., Piedade, M.S., 2017. IEEE Trans. Biomed. Circuits Syst. 11, 988–1000.
De Boer, B.M., Kahlman, J., Jansen, T., Duric, H., Veen, J., 2007. Biosens. Bioelectron. 22, 2366–2370.
Dias, T.M., Cardoso, F.A., Martins, S.A.M., Martins, V.C., Cardoso, S., Gaspar, J.F., Monteiro, G., Freitas, P.P., 2016. Anal. Methods 8, 119–128.
Gaster, R.S., Hall, D.A., Nielsen, C.H., Osterfeld, S.J., Yu, H., Mach, K.E., Wilson, R.J., Murmann, B., Liao, J.C., Gambhir, S.S., 2009. Nat. Med. 15, 1327.
Goh, D., Kong, K.V., Jayakumar, P., Gong, T., Dinish, U.S., Olivo, M., 2016. J. Mol. Eng. Mater. 4, 1640011.
Hall, D.A., Gaster, R.S., Lin, T., Osterfeld, S.J., Han, S., Murmann, B., Wang, S.X., 2010. Biosens. Bioelectron. 25, 2051–2057.
Jayson, G.C., Kohn, E.C., Kitchener, H.C., Ledermann, J.A., 2014. Lancet 384, 1376–1388.
Jing, Y., He, S., Kline, T., Xu, Y., Wang, J.-.P., 2009. Engineering in medicine and biology society. EMBC 2009. In: Proceedings of the Annual International Conference of the IEEE. IEEE, pp. 4483–4486.
Krishna, V.D., Wu, K., Perez, A.M., Wang, J.P., 2016. Front. Microbiol. 7, 8.
Li, Y., Srinivasan, B., Jing, Y., Yao, X., Hugger, M.A., Wang, J.-P., Xing, C., 2010. J. Am. Chem. Soc. 132, 4388–4392.
Makawita, S., Diamandis, E.P., 2010. Clin. Chem. 56, 212–222.
Matz, M., Coleman, M.P., Carreira, H., Salmerón, D., Chirlaque, M.D., Allemani, C., Group, C.W., 2017. Gynecol. Oncol. 144, 396–404.
Moore, R.G., McMeekin, D.S., Brown, A.K., DiSilvestro, P., Miller, M.C., Allard, W.J., Gajewski, W., Kurman, R., Bast, R.C., Skates, S.J., 2009. Gynecol. Oncol. 112, 40–46.
Oza, A.M., Cook, A.D., Pfisterer, J., Embleton, A., Ledermann, J.A., Pujade-Lauraine, E., Kristensen, G., Carey, M.S., Beale, P., Cervantes, A., 2015. Lancet Oncol. 16, 928–936.
Rifai, N., Gillette, M.A., Carr, S.A., 2006. Nat. Biotechnol. 24, 971–983.
Rossetti, C., Świtnicka-Plak, M.A., Halvorsen, T.G., Cormack, P.A.G., Sellergren, B., Reubsaet, L., 2017. Sci. Rep. 7, 44298.
Siegel, R.L., Miller, K.D., Jemal, A., 2016. CA A Cancer J. Clin. 66, 7–30.
Srinivasan, B., Li, Y., Jing, Y., Xing, C., Slaton, J., Wang, J.-P., 2011. Anal. Chem. 83, 2996–3002.
Srinivasan, B., Li, Y., Jing, Y., Xu, Y., Yao, X., Xing, C., Wang, J., 2009. Angew. Chem. Int. Ed. 48, 2764–2767.
Su, Z., Graybill, W.S., Zhu, Y., 2013. Clin. Chim. Acta 415, 341–345.
Ueland, F.R., 2017. Diagnostics 7, 14.
Wang, W., Wang, Y., Tu, L., Klein, T., Feng, Y., Li, Q., Wang, J.-P., 2014. Anal. Chem. 86, 3712–3716.
Wang, W., Wang, Y., Tu, L., Klein, T., Feng, Y., Wang, J.-P., 2013. IEEE Trans. Magn. 49, 296–299.
Wang, Y., Wang, W., Yu, L.N., Tu, L., Feng, Y.L., Klein, T., Wang, J.P., 2015. Biosens. Bioelectron. 70, 61–68.
Wu, K., Klein, T., Krishna, V.D., Su, D., Perez, A.M., Wang, J.-P., 2017. ACS Sens. 2, 1594–1601.
Yang, W.-L., Lu, Z., Bast Jr, R.C., 2017. Expert Rev. Mol. Diagn. 17, 577–591.
Zhi, X., Liu, Q.S., Zhang, X., Zhang, Y.X., Feng, J., Cui, D.X., 2012. Lab Chip 12, 741–745.